Neurobiology of Disease

Cell- and Pathway-Specific Disruptions in the Accumbens of Fragile X Mouse

Gabriele Giua,[1,2] Jessica Pereira-Silva,[1,2] Alba Caceres-Rodriguez,[1,2] Olivier Lassalle,[1,2] Pascale Chavis,[1,2] and Olivier J. Manzoni[1,2]

[1]Institut de neurobiologie de la méditerranée, Institut National de la Santé et de la Recherche Médicale U1249, Marseille 13273, France and [2]Aix-Marseille University, Marseille 13284, France

Fragile X syndrome (FXS) is a genetic cause of intellectual disability and autism spectrum disorder. The mesocorticolimbic system, which includes the prefrontal cortex (PFC), basolateral amygdala (BLA), and nucleus accumbens core (NAcC), is essential for regulating socioemotional behaviors. We employed optogenetics to compare the functional properties of the BLA→NAcC, PFC→NAcC, and reciprocal PFC↔BLA pathways in *Fmr1−/y::Drd1a-tdTomato* male mice. In FXS mice, the PFC↔BLA reciprocal pathway was unaffected, while significant synaptic modifications occurred in the BLA/PFC→NAcC pathways. We observed distinct changes in D1 striatal projection neurons (SPNs) and separate modifications in D2 SPNs. In FXS mice, the BLA/PFC→NAcC-D2 SPN pathways demonstrated heightened synaptic strength. Focusing on the BLA→NAcC pathway, linked to autistic symptoms, we found increased AMPAR and NMDAR currents and elevated spine density in D2 SPNs. Conversely, the amplified firing probability of BLA→NAcC-D1 SPNs was not accompanied by increased synaptic strength, AMPAR and NMDAR currents, or spine density. These pathway-specific alterations resulted in an overall enhancement of excitatory-to-spike coupling, a physiologically relevant index of how efficiently excitatory inputs drive neuronal firing, in both BLA→NAcC-D1 and BLA→NAcC-D2 pathways. Finally, the absence of fragile X messenger ribonucleoprotein 1 (FMRP) led to impaired long-term depression specifically in BLA→D1 SPNs. These distinct alterations in synaptic transmission and plasticity within circuits targeting the NAcC highlight the potential role of postsynaptic mechanisms in selected SPNs in the observed circuit-level changes. This research underscores the heightened vulnerability of the NAcC in the context of FMRP deficiency, emphasizing its pivotal role in the pathophysiology of FXS.

Key words: **basolateral amygdala; fragile X syndrome; mesocorticolimbic system; nucleus accumbens; prefrontal cortex; synaptic function**

Significance Statement

Fragile X syndrome (FXS) is a neurodevelopmental disorder characterized by significant emotional dysregulation and social challenges. The mesocorticolimbic system is a key socioemotional regulator. Nevertheless, its functioning in this condition is still poorly understood. Our study investigates connections between the basolateral amygdala (BLA), prefrontal cortex (PFC), and nucleus accumbens core (NAcC). We observed that while the PFC↔BLA reciprocal connections remained unaffected, their projections onto the NAcC showed target cell-specific changes. Specifically, D2 striatal projection neurons (SPNs) exhibited increased synaptic transmission and spine density, whereas D1 SPNs showed heightened firing probability and impaired long-term depression, alongside enhanced neuronal firing efficiency in both SPN types. These findings emphasize the NAcC's crucial role as a neurobiological substrate in the pathophysiology of FXS.

Received Aug. 22, 2023; revised May 9, 2024; accepted May 16, 2024.

Author contributions: G.G., J.P-S., P.C., and O.J.M. designed research; G.G., J.P-S., A.C-R., and O.L. performed research; G.G., J.P-S., and O.L. analyzed data; G.G. and O.J.M. wrote the paper.

This work was supported by the Institut National de la Santé et de la Recherche Médicale (INSERM), ANR 2CureXFra (ANR- 18-CE12-0002-01), and the Fondation Jérôme Lejeune ("A new view in neurophysiological and socio-communicative deficits of Fragile X"). We are grateful to the Chavis-Manzoni team members for their helpful discussions.

The authors declare no competing financial interests.

Correspondence should be addressed to Olivier J. Manzoni at olivier.manzoni@inserm.fr.

https://doi.org/10.1523/JNEUROSCI.1587-23.2024

Introduction

Fragile X syndrome (FXS) is a prominent neurodevelopmental disorder and a leading monogenic cause of inherited intellectual disability and autism spectrum disorder (Hunter et al., 2014; Wiśniowiecka-Kowalnik and Nowakowska, 2019). Affecting ~1.4 out of every 10,000 males and 0.9 out of every 10,000 females (Hunter et al., 2014), FXS results from the transcriptional silencing of the *FMR1* gene on the X chromosome, causing deficient expression of fragile X messenger ribonucleoprotein 1

(FMRP). This FXS results in neurodevelopmental abnormalities causing disruptions in neuronal excitability and circuitry. These disruptions ultimately contribute to the cognitive and behavioral impairments observed in individuals with FXS (Contractor et al., 2015). Many aspects of FXS remain poorly understood, particularly regarding the specific brain circuits and synaptic dysfunctions that contribute to the dysregulation of emotional processing, appropriate behavioral responses, and decision-making in socially rewarding contexts.

The prefrontal cortex (PFC), basolateral amygdala (BLA), and nucleus accumbens core (NAcC) are interconnected components of the mesocorticolimbic network that regulate socioemotional behaviors. The NAcC acts as a central hub (Supekar et al., 2018; Pfaff and Barbas, 2019), integrating emotional, motivational, and reward/aversion signals (Bromberg-Martin et al., 2010; Floresco, 2015). Dopamine receptor 1-expressing and dopamine receptor 2-expressing striatal projection neurons (SPNs) within the NAcC have distinct roles in processing information in healthy conditions and various disorders (Lobo and Nestler, 2011; Francis et al., 2015). The absence of FMRP significantly impacts the intrinsic properties of SPNs and NAcc's synapses (Jung et al., 2012; Neuhofer et al., 2015, 2018; Giua et al., 2023); however, circuit-level information are lacking.

Excitatory synapses from the BLA onto SPNs carry crucial information regarding the emotional valence of stimuli and guide action selection in reward-related contexts (Sharp, 2017; Bercovici et al., 2018). Activation of the BLA→NAcC pathway impairs motivation for social interaction, reduces social preference, and induces social avoidance in typical mice (Folkes et al., 2020), while inhibiting this pathway restores sociability in the *Shank3B*$^{-/-}$ mouse model of autism (Folkes et al., 2020). The involvement of the PFC→NAcC pathway in effort-related decision-making and social avoidance, as well as the role of the reciprocal PFC↔BLA connection in processing information, emotional balance, and cognitive control, aligns with the hypothesis that this interconnected neural network may underlie the distinctive behavioral phenotype observed in FXS (Christakou et al., 2004; Block et al., 2007; Hauber and Sommer, 2009; Vialou et al., 2014; Amadei et al., 2017; Murray and Fellows, 2022; Leduke et al., 2023).

To test this idea, we conducted a comprehensive study utilizing ex vivo electrophysiology, optogenetics, and the *Fmr1−/y::Drd1a-tdTomato* mouse model to examine the synaptic functioning of the PFC, BLA, and NAcC network in FXS. The findings reveal a high level of circuit specificity for synaptic alterations induced by FMRP deficiency. While the reciprocal PFC↔BLA remained unaffected, their inputs onto the NAcC exhibit pathway- and target cell-specific changes in synaptic transmission and plasticity. These modifications primarily manifest in a postsynaptic-dependent manner, underscoring the NAcC as a significant neurobiological substrate in the pathophysiology of FXS.

Materials and Methods

Animals. Animals were treated in compliance with the European Communities Council Directive (86/609/EEC) and the United States National Institutes of Health Guide for the care and use of laboratory animals. The French Ethical Committee authorized this project (APAFIS#3279-2015121715284829 v5). Mice were obtained breeding *Drd1a-tdTomato* × *Fmr1* KO2 mice from the Jackson Laboratory (stock #016204) and FRAXA Research Foundation, respectively. Both strains had a C57Bl/6J background. Mice were acclimated to the animal facility for 1 week and then housed in male *Drd1a-tdTomato* and female *Fmr1+/−* pairs for breeding. Pups were weaned and ear tagged for identification and genotyping at Postnatal Day (PND) 21. Experiments were performed on first-generation male mice between PND 70 and PND 100. *Fmr1+/y::Drd1a-tdTomato* mice composed the control group [wild type (WT)] and *Fmr1−/y::Drd1a-tdTomato* the experimental group [knock-out (KO)]. Mice were housed in groups of 4–5 at constant room temperature (20 ± 1°C) and humidity (60%) and exposed to a light cycle of 12 h light/dark with *ad libitum* access to food and water.

Stereotaxic surgery. Ten microliter Hamilton syringe with microinjection needles (32 G) was connected to an infusion/withdraw pump (KD Scientific Legato 130) and filled with purified, concentrated adeno-associated virus (2.2×10^{13} GC/ml) encoding hChR2-EYFP under control of the CaMKIIα promoter [pAAV-CaMKIIa-hChR2(H134R)-EYFP, Addgene 26969-AAV9].

Adolescent male mice (PND 40–50) were deeply anesthetized with isoflurane and treated with carprofen (5 mg/Kg, s.c.) before placing them in a stereotaxic frame. Microinjection needles were bilaterally placed into the BLA (coordinates from the bregma: AP, −1.2 mm; ML, ±3.1 mm; DV, 4.8 mm) or PFC (AP, 2 mm; ML, ±0.3 mm; DV, 2.2 mm), and 250 nl of virus was injected with a speed of 100 nl/min. The needles were left in place for an additional 5 min to allow for diffusion of virus particles away from the injection site.

Slice preparation for ex vivo electrophysiological recordings. Between 4 and 6 weeks after stereotaxic surgery, adult male mice were deeply anesthetized with isoflurane and decapitated according to institutional regulations. The brain was sliced (300 µm) on the coronal plane with a vibratome (Integraslice, Campden Instruments) in a sucrose-based solution at 4°C containing the following (in mM): 87 NaCl, 75 sucrose, 25 glucose, 2.5 KCl, 4 $MgCl_2$, 0.5 $CaCl_2$, 23 $NaHCO_3$, and 1.25 NaH_2PO_4. Immediately after cutting, slices were stored for 1 h at 32°C in a low-calcium artificial cerebrospinal fluid (ACSF) containing the following (in mM), 130 NaCl, 11 glucose, 2.5 KCl, 2.4 $MgCl_2$, 1.2 $CaCl_2$, 23 $NaHCO_3$, and 1.2 NaH_2PO_4, equilibrated with 95% O_2/5% CO_2. After 1 h of recovery, slices were kept at room temperature until the time of recording.

Electrophysiology. Whole-cell patch–clamp and extracellular field recordings were made from mouse coronal slices containing the PFC, BLA, and NAcC. Brain slices were placed in the recording chamber and superfused at 2 ml/min with normal-calcium ACSF, containing the following (in mM), 130 NaCl, 11 glucose, 2.5 KCl, 1.2 $MgCl_2$, 2.4 $CaCl_2$, 23 $NaHCO_3$, and 1.2 NaH_2PO_4, for recordings in BLA and NAcC and low-calcium ACSF for those in PFC, equilibrated with 95% O_2/5% CO_2. The superfusion medium contained gabazine 10 µM (SR 95531 hydrobromide; Tocris Bioscience) to block GABA type A receptors. Recordings were performed at 25 ± 1°C in the NAcC and 32 ± 1°C in PFC and BLA.

For whole-cell patch–clamp experiments, medial NAcC SPNs were visualized using an upright microscope with infrared illumination and then distinguished based on the visualization of *Drd1-tdTomato* using fluorescent illumination. Given that in this specific mouse strain, the coexpression of D1 and D2 receptors in SPNs is relatively low (ranging from ∼1.9% in the dorsal striatum to ∼7. 3% in the NAc core; Gagnon et al., 2017), it can be reasonably assumed that almost all *Drd1-tdTomato*-positive neurons are D1 SPNs and those *tdTomato*-unlabeled are D2 SPNs. Therefore, for ease of understanding, we use the nomenclature D1 and D2 SPNs along this study recognizing that this classification is tentative.

The intracellular solution was based on K-gluconate containing the following (in mM), 145 K-gluconate, 3 NaCl, 1 $MgCl_2$, 1 EGTA, 0.3 $CaCl_2$, 2 Na_2ATP, 0.5 NaGTP, 0.2 cAMP, 10 buffered with HEPES, except in the AMPAR/NMDAR ratio experiments where it was based on $CsMeSO_3$ that contains the following (in mM): 143 $CsMeSO_3$, 5 NaCl, 1 $MgCl_2$, 1 EGTA, 0.3 $CaCl_2$, 10 HEPES, 2 Na_2ATP, 0.3 NaGTP, and 0.2 cAMP. Their pH was adjusted to 7.2 and osmolarity to 290–300 mOsm. Electrode resistance was 2–4 MΩ. Access resistance compensation was not used, and acceptable access resistance was

<30 MOhms. The potential reference of the amplifier was adjusted to zero prior to breaking into the cell. In V-clamp experiments, a −2 mV hyperpolarizing pulse was applied before each optically evoked excitatory postsynaptic currents (oEPSCs) to evaluate the access resistance, and those experiments in which this parameter changed >25% were rejected. oEPSCs were recorded at −70 mV except where differentially indicated. Input–output (I–O) experiments were made by recording the response to increasing optical stimulation intensity (0–6 mW, steps of 0.5 mW). AMPAR/NMDAR ratios were calculated on the area (pA * ms) of oEPSCs (having AMPAR and NMDAR components) at +40 mV. The AMPAR component was isolated by bath application of an NMDAR antagonist (APV; 50 μM, Tocris Bioscience). NMDAR component was obtained by digital subtraction of the AMPAR-oEPSC from the dual component (Kasanetz and Manzoni, 2009). The optically evoked excitatory postsynaptic potential (oEPSP)–spike coupling (ES coupling) experiments were performed in I-clamp maintaining the membrane potential at −65 mV. Ten traces were recorded for each step of increasing stimulus intensity (0–6 mW, steps of 0.5 mW), obtaining the mean slope and mean spike probability for each step. oEPSP slopes were measured during the first 2 ms, sorted in 0.5 mV/ms bins, and the firing probability was determined for each bin. For long-term depression (LTD) experiments, baseline stimulation frequency was set at 0.1 Hz, and plasticity was induced by 10 min at 10 Hz stimulation (10′–10 Hz). The intensity of optical stimulation was set at 60% of that required to achieve a maximum response performing an I–O curve (0–6 mW, steps of 0.5 mW). Previous studies have shown that 10′–10 Hz synaptic stimulation activates mGlu5 receptors leading to endocannabinoid-mediated LTD in multiple brain areas (Lafourcade et al., 2007; Puente et al., 2011; Jung et al., 2012). Paired Pulse Ratio (PPR) was determined by calculating the ratio (P2/P1) of the amplitudes of two oEPSCs, elicited with a 50 ms interval between them.

For extracellular field recordings, the PFC, BLA, and NAcC were visualized using an upright microscope with infrared illumination. Extracellular oEPSPs were recorded in the medial prelimbic PFC, basal BLA, and medial NAcC with an ACSF-filled electrode. I–O and LTD experiments were conducted as described above. The glutamatergic nature of oEPSPs was systematically confirmed at the end of the experiments using the ionotropic glutamate receptor antagonist cyanquixaline (20 μM; NIH), which specifically blocked the synaptic component without altering the nonsynaptic component (data not shown).

Optogenetic. Optical stimulation was performed with a 473 nm laser (Dragon Lasers) coupled to a 50 μm core glass silica optical fiber (Thorlabs) positioned directly above the slice orientated at 30° ∼350 μm from the recording electrode. At the site of recording discounting scattering a region of ∼0.05 mm^2 was illuminated that after power attenuation due to adsorption and scattering in the tissue was calculated as ∼100 mW/mm^2 (Yizhar et al., 2011). Optically evoked responses were obtained every 10 s with pulses of 473 nm wavelength light (0–10 mW, 2 ms). The stimulating optical fiber was positioned dorsomedial to the recording electrode.

Electrophysiological data acquisition and analysis. All recordings were collected using an Axopatch-200B amplifier (Axon Instruments, Molecular Devices); data were low-pass filtered at 2 kHz, digitized (10 kHz, DigiData 1440A, Axon Instruments), acquired using Clampex 10.7, and analyzed using Clampfit 11.2 (Molecular Devices).

Dendritic spines' reconstruction and quantification. The method to label and analyze dendrites and spines was adapted from our previous publications (Iafrati et al., 2014; Guily et al., 2022). To label the SPNs, we loaded the neurobiotin (NB) into the neurons via patch pipettes containing a $CsMeSO_3$+ NB-based intracellular solution. The brain slices were then fixed overnight using 4% paraformaldehyde, rinsed with PBS, and subsequently incubated overnight at 4°C with streptavidin–Alexa Fluor 555 (diluted at 1:200 in PBS). Following this, the slices were prepared for confocal imaging. Only neurons with adequately filled dendritic trees were included in the analysis. Two to five third- and fourth-order dendrites per neuron were selected for analysis. For each dendrite, the first and last 10% in length were excluded from the analysis. Confocal stack images were acquired using a Zeiss LSM-800 confocal microscope equipped with a Plan-Apochromat 63× oil-immersion objective (NA, 1.4). The frame size was set at 1,024 × 1,024 pixel (pixel size, 0.07 × 0.07; *z*-step, 0.12) with a 1.4× scan zoom. Laser power and photomultiplier gain were adjusted using the range indicator function, ensuring that the most intense pixels remained just below saturation. To compensate for spherical aberration and correct *z*-smear for reliable spine morphology, a tridimensional deconvolution of each stack was performed using the Zeiss 2.6 deconvolution plug-in (fast iterative, Richardson–Lucy method).

Tridimensional reconstruction and semiautomated analysis were carried out using the Imaris software (Bitplane).

Statistics. Statistical analyses were conducted using the Prism software (GraphPad Software 9), employing tests specified in the main text of figure legends or Extended Data Tables. The data were initially assessed for normality using the Shapiro–Wilk test and screened for outliers using the ROUT test. Subsequently, most of the data were subjected to unpaired/paired *t* tests or two-way ANOVA (with genotype and cell type as main factors), followed by Tukey's multiple-comparison tests. ES coupling data were analyzed using the extra sum-of-squares *F* test method to compare curves based on half-maximal probability factor. Complete statistical details can be found in the Extended Data Tables. In the figures and tables, "*N*" and "*n*" values represent individual animals and individual cells, respectively, except in the case of dendritic spine analysis where they refer to individual cells and individual dendrites, respectively. Statistical significance was set at $p < 0.05$.

Results

The objective of this study was to explore the intricate synaptic circuitry involving the PFC, BLA, and NAcC and to uncover potential neurophysiological mechanisms that underlie the emotional and behavioral changes observed in individuals with FXS. To achieve this, we employed a combination of patch-clamp/extracellular electrophysiology and optogenetic techniques to examine the BLA→NAcC and PFC→NAcC connections, as well as the reciprocal PFC↔BLA connection in *Fmr1-/y::Drd1a-tdTomato* FXS mice.

Within the PFC-BLA-NAcC network of FMRP-deficient mice, there is a specific enhancement of synaptic transmission at the inputs onto the NAcC

The significance of the PFC-BLA-NAcC excitatory network in emotional regulation, behavior selection, and decision-making processes has motivated us to investigate the strength of synaptic transmission at the reciprocal PFC↔BLA, BLA→NAcC, and PFC→NAcC synapses in both WT and FXS mice. To achieve this, we conducted experiments comparing excitatory synaptic transmission at these four synapses in our FXS mouse model. We recorded extracellular field responses while incrementally increasing optical stimulation in the axon terminal zones. The resulting I–O curves revealed distinct effects: the absence of FMRP did not affect PFC↔BLA synapses (Fig. 1*A–F*, Extended Data Tables 1-1, 1-2), whereas it led to a significant enhancement of synaptic strength in the BLA→NAcC and PFC→NAcC connections when compared with WT littermates (Fig. 1*G–L*, Extended Data Tables 1-3, 1-4).

FMRP deficiency specifically increases BLA/PFC→D2 SPNs glutamatergic transmission

Considering the specific impact of FMRP deficiency on distinct cell subtypes within NAcC's principal neurons (as observed in Giua et al., 2023), we determined the consistency of enhanced BLA→NAcC and PFC→NAcC synaptic transmission across

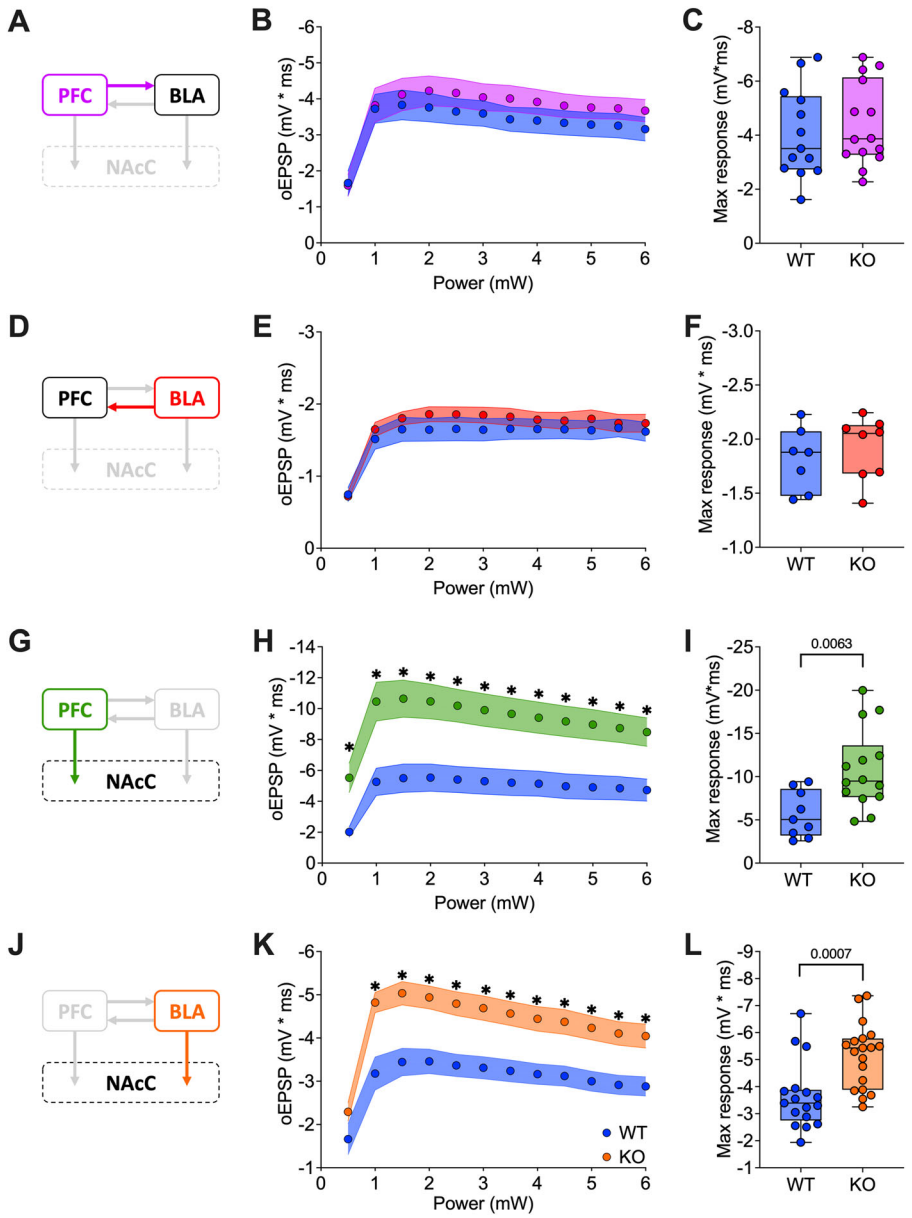

Figure 1. Enhanced synaptic transmission at NAcC inputs in FMRP-deficient mice within the PFC-BLA-NAcC network. ***A***, ***D***, ***G***, ***J***, Schematic representation of the interconnections between PFC, BLA, and NAcC with the individual pathways examined highlighted. ***B***, ***C***, ***E***, ***F***, ***H***, ***I***, ***K***, ***L***, In FXS mice, the absence of FMRP does not impact synaptic transmission in the PFC→BLA (***B***, ***C***) and BLA→PFC (***E***, ***F***) connections while leading to increased transmission in the PFC→NAcC (***H***, ***I***) and BLA→NAcC (***K***, ***L***) pathways, as indicated by extracellular oEPSP recordings evoked by increasing light stimulation. ***B***, ***E***, ***H***, ***K***, A single dot represents group mean value at that stimulation intensity step. Data are shown as mean ± SEM in the *XY* plot. Unpaired *t* tests, **p* values <0.05. ***C***, ***F***, ***I***, ***L***, A single dot represents an individual mouse. Data are shown as the min. to max. box plot with median and 25–75 percentile. Unpaired *t* tests. *P* values <0.05 are displayed in graphs. ***B***, ***C***, WT $N = 13$ in blue, KO $N = 14$ in purple. ***E***, ***F***, WT $N = 7$ in blue, KO $N = 8$ in red. ***H***, ***I***, WT $N = 9$ in blue, KO $N = 14$ in green. ***K***, ***L***, WT $N = 17$ in blue, KO $N = 19$ in orange. Full statistics are provided in Extended Data Tables 1-1–1-4.

synapses involving D1 or D2 SPNs (Figs. 2, 3). Using whole-cell recordings to construct an opto-I–O curve, our findings demonstrated distinct synaptic strength patterns in WT animals with greater synaptic transmission from the BLA to D1 SPNs compared with D2 SPNs (Fig. 2*B*, Extended Data Table 2-1). However, this divergence was not observed in KO mice lacking FMRP (Fig. 2C, Extended Data Table 2-2). The genotype difference arose because there is no change in synaptic strength at BLA→D1 SPN synapses (Fig. 2*D*, Extended Data Table 2-3), while there was an increase in synaptic transmission specifically at BLA→D2 SPNs synapses (Fig. 2*E*, Extended Data Table 2-4).

Furthermore, a similar pattern of enhanced synaptic strength was observed at the PFC→NAcC connection. Opto-I–O curves demonstrated distinct synaptic strengths in WT animals, with stronger transmission from the PFC to D1 SPNs compared with D2 SPNs (Fig. 3*B*, Extended Data Table 3-1), but not in KOs (Fig. 3C, Extended Data Table 3-2). Indeed, in mice lacking FMRP, there was an augmentation of synaptic efficacy specifically at the PFC→D2 SPNs synapses (Fig. 3*E*, Extended Data Table 3-4), while PFC→D1 SPN synapses remained unchanged (Fig. 3*D*, Extended Data Table 3-3). Therefore, in the absence of FMRP, both accumbal inputs from the PFC and BLA exhibit increased synaptic transmission selectively with D2 SPNs.

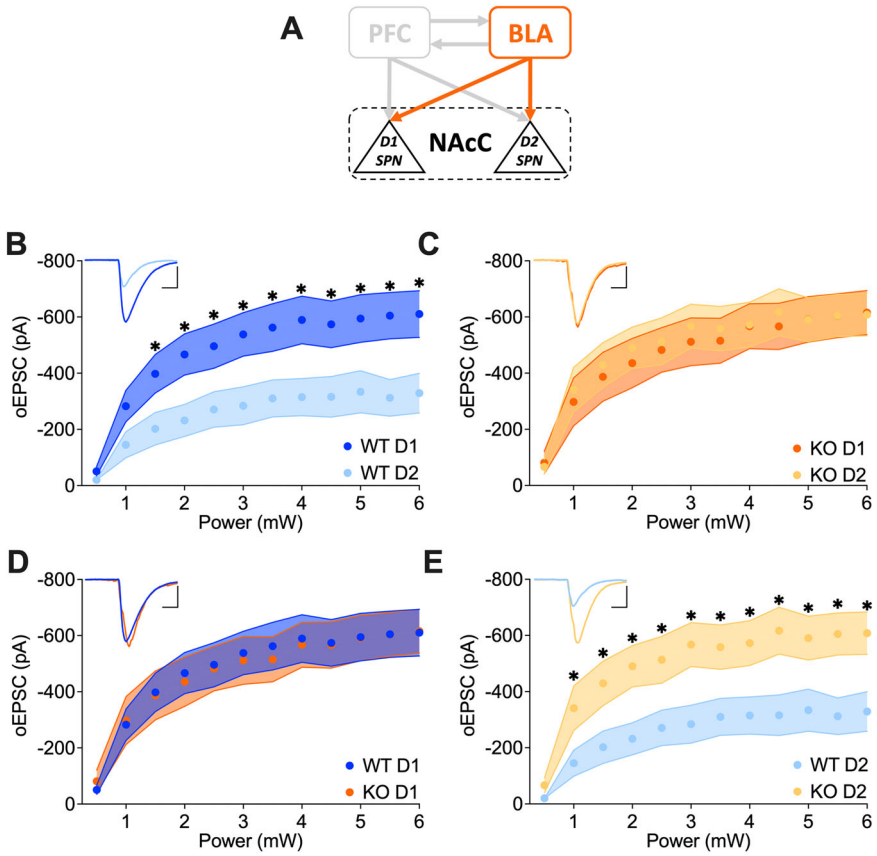

Figure 2. Increased glutamatergic transmission at BLA→D2 SPNs in FMRP-deficient mice. ***A***, Schematic representation illustrating the interconnections between PFC-BLA-NAcC and emphasizing the specific BLA-NAcC (D1/D2 SPNs) pathway under scrutiny. ***B***, ***C***, Whole-cell recordings reveal that while in *Fmr1* WT the BLA synaptic transmission in NAcC is stronger toward D1 than D2 SPNs, in KO it is equal. ***D***, ***E***, BLA→D2 SPN synaptic transmission is increased in the absence of FMRP but not that of BLA→D1 SPNs. ***B–E***, A single dot represents group mean value at that stimulation intensity step. Data are shown as mean ± SEM in the *XY* plot. Unpaired *t* tests, **p* values <0.05. Example trace in the top left; scale bar: 10 ms, 200 pA. WT D1 SPNs $N = 14$ ($n = 18$) in dark blue, WT D2 SPNs $N = 13$ ($n = 16$) in light blue, KO D1 SPNs $N = 12$ ($n = 13$) in dark orange, KO D2 SPNs $N = 10$ ($n = 12$) in light orange. Full statistics are provided in Extended Data Tables 2-1–2-4.

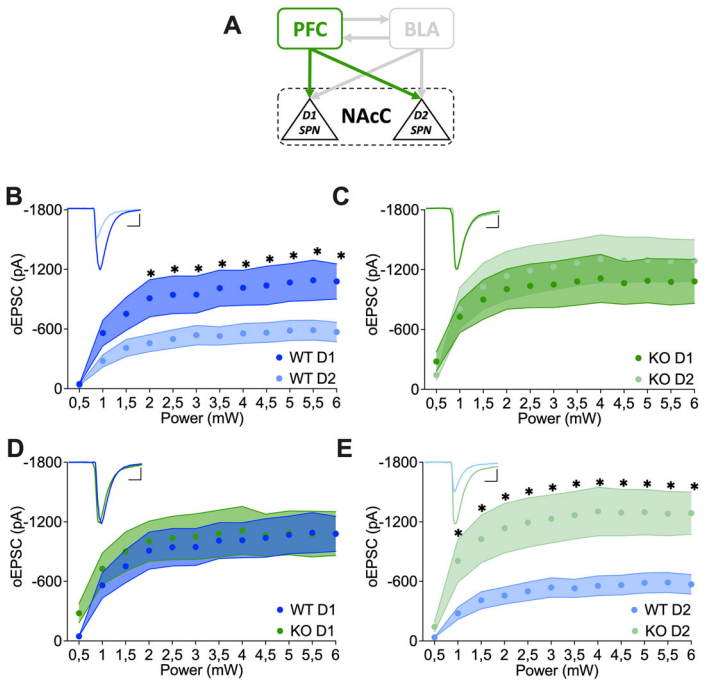

Figure 3. Increased glutamatergic transmission at PFC→D2 SPNs in FMRP-deficient mice. ***A***, Schematic representation illustrating the interconnections between PFC-BLA-NAcC and emphasizing the specific PFC-NAcC (D1/D2 SPNs) pathway under scrutiny. ***B***, ***C***, Whole-cell recordings reveal that while in *Fmr1* WT the PFC synaptic transmission in NAcC is stronger toward D1 than D2 SPNs, in KO it is equal. ***D***, ***E***, PFC→D2 SPN synaptic transmission is increased in the absence of FMRP but not that of PFC→D1 SPNs. ***B–E***, A single dot represents group mean value at that stimulation intensity step. Data are shown as mean ± SEM in the *XY* plot. Unpaired *t* tests, **p* values <0.05. Example trace in the top left, scale bar: 10 ms, 200 pA. WT D1 SPNs $N = 8$ ($n = 9$) in dark blue, WT D2 SPNs $N = 8$ ($n = 8$) in light blue, KO D1 SPNs $N = 10$ ($n = 11$) in dark green, KO D2 SPNs $N = 9$ ($n = 10$) in light green. Full statistics are provided in Extended Data Tables 3-1–3-4.

Given the crucial role of the BLA-NAcC pathway in regulating autistic symptoms (Folkes et al., 2020), we opted to thoroughly examine and investigate this pathway in the subsequent phases of our study.

Enhancement of BLA→D2 SPNs synaptic transmission in the NAcC due to FMRP deficiency: increased AMPAR and NMDAR currents

To gain insight into the potential mechanisms underlying the altered BLA→NACc transmission, we conducted an evaluation of the AMPA and NMDA receptor components in both target cell types (Fig. 4). The analysis revealed that the absence of FMRP resulted in an increase in both AMPAR and NMDAR currents exclusively at BLA→D2 SPN synapses, while BLA→D1 SPN synapses remained unaffected (Fig. 4*C*,*D*, Extended Data Table 4-1). We calculated the AMPAR/NMDAR ratio, an indicator of the balance between synaptic connection strength and potential plasticity. In WT animals, a notable difference was observed: synapses formed by the BLA with D1 SPNs exhibited a lower AMPAR/NMDAR ratio compared with BLA→D2 SPN synapses (Fig. 4*E*, Extended Data Table 4-1). However, this divergence disappeared in the absence of FMRP (Fig. 4*E*, Extended Data Table 4-1). Overall, these findings suggest that FMRP deficiency selectively enhances BLA→D2 SPN synaptic transmission in the NAcC by increasing both AMPAR and NMDAR currents.

FMRP absence impacts synaptic integration and action potential generation in BLA→NAcC synapses

ES coupling, in other words the transformation of synaptic excitation into an action potential (EPSP–spike conversion), ultimately governs neuronal responsiveness (Daoudal et al., 2002). In FXS, it has been established that there are changes in intracellular excitability within the NAcC (Giua et al., 2023). Additionally, the current findings indicate pathway-specific alterations in synaptic strength. However, it remains unclear whether active synaptic integration is affected in FXS. We examined the impact of FMRP's absence on the integration functionality at BLA→NAcC synapses (Fig. 5). Stepwise increase in optical stimulation was applied to explore the likelihood of action potential generation resulting from the synaptically induced depolarization of SPNs at BLA→NAcC connections (Fig. 5*A*). First, plotting the probability of firing against the oEPSP slope allowed the evaluation of whether FMRP influences the probability of action potential generation at the same magnitude of depolarization, thus excluding the influence of variable synaptic strengths. Intriguingly, in WT mice, an opposition emerged, wherein D2 SPNs exhibited a higher probability of generating action potentials, compared with D1 SPNs at the same oEPSP magnitude (Fig. 5*C*, Extended Data Table 5-1). However, in FXS mice, both types of synapses demonstrated similar probabilities of inducing action potentials (Fig. 5*D*, Extended Data Table 5-1). Analyses per cell type revealed that this discrepancy between the two genotypes stemmed from the fact that the absence of FMRP increased the firing probability in D1 SPNs (Fig. 5*E*, Extended Data Table 5-1), but not in D2 SPNs (Fig. 5*F*, Extended Data Table 5-1).

Next the relationship between synaptic strength and firing probability was examined in BLA→NAcC synapses of both genotypes. Thus, the firing probability of SPNs was plotted against the intensity of optical stimulation. We found that D2 SPNs achieved half-maximal probability at lower stimulation intensities compared with D1 SPNs in both genotypes (Fig. 5*G*,*H*, Extended Data Table 5-2). Interestingly, in the absence of FMRP, both D1 and D2 SPNs attained half-maximal probability at lower intensities than their WT counterparts (Fig. 5*I*,*J*, Extended Data Table 5-2). Collectively, these findings demonstrate that in FXS animals, in contrast to WTs, the activation of BLA→NAcC synapses is more likely to result in action potential generation in both D1 and D2 SPNs.

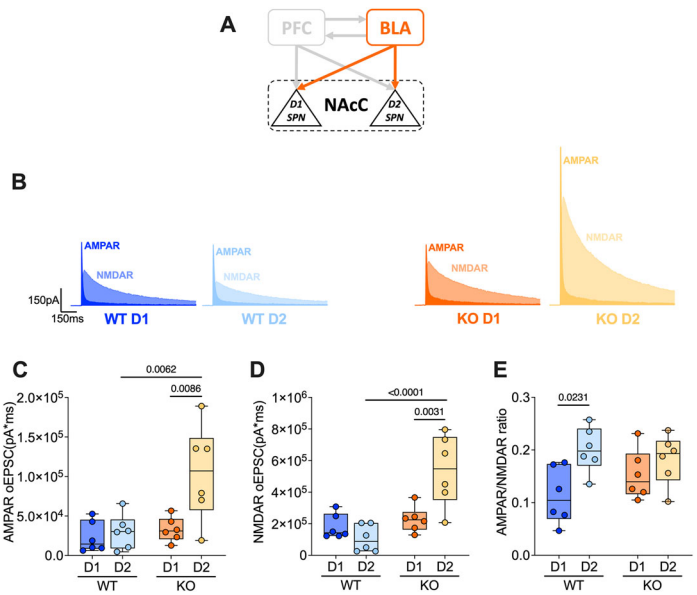

Figure 4. FMRP absence increases both AMPAR and NMDAR currents at BLA→D2 SPN synapses. ***A***, Schematic representation illustrating the interconnections between PFC-BLA-NAcC and emphasizing the specific BLA-NAcC (D1/D2 SPNs) pathway under scrutiny. ***B***, Example traces of AMPAR and NMDAR currents resulting from optical stimulation of BLA→SPNs synapses in *Fmr1* WT and KO littermates. ***C***, ***D***, AMPAR and NMDAR oEPSCs are higher in BLA→D2 SPNs in the absence of FMRP. ***E***, AMPAR/NMDAR ratio differs between D1 and D2-SPNs in WTs but not in KOs. ***C–E***, A single dot represents an individual mouse. Data are shown as the min. to max. box plot with median and 25–75 percentile. Two-way ANOVA followed by Tukey's multiple-comparison test. *P* values <0.05 are displayed in graphs. WT D1 SPNs $N = 6$ ($n = 7$) in dark blue, WT D2 SPNs $N = 6$ ($n = 7$) in light blue, KO D1 SPNs $N = 6$ ($n = 9$) in dark orange, KO D2 SPNs $N = 6$ ($n = 9$) in light orange. Full statistics are provided in Extended Data Table 4-1.

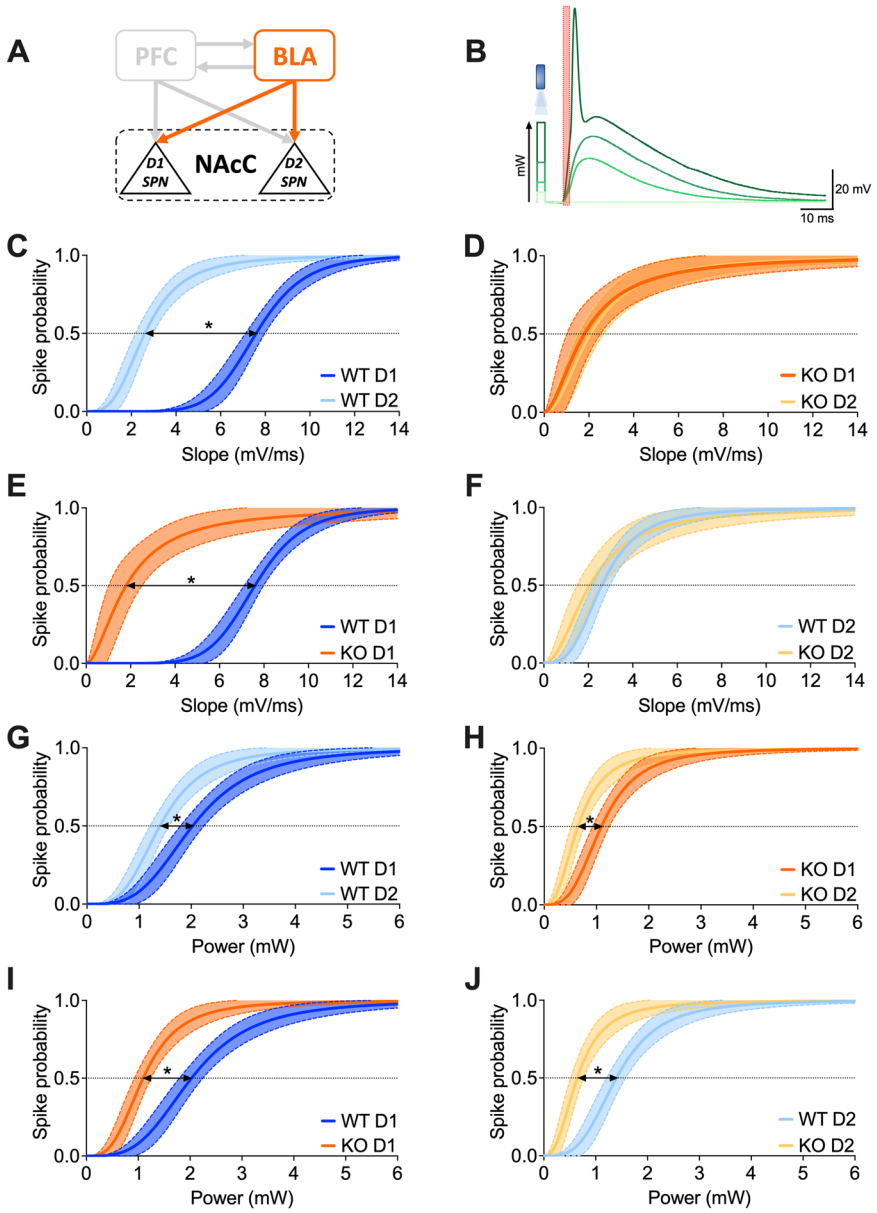

Figure 5. The firing probability of D1 and D2 SPNs stimulated from the BLA is higher in the absence of FMRP. ***A***, Schematic representation illustrating the interconnections between PFC-BLA-NAcC and emphasizing the specific BLA-NAcC (D1/D2 SPNs) pathway under scrutiny. ***B***, Example traces demonstrate that depolarization amplitude increases with optical stimulation intensity until the action potential threshold is reached; the red box indicates the slope extrapolation interval. ***C***, ***D***, In *Fmr1* WT mice, stimulating BLA→NAcC synapses, there is a higher probability of triggering an action potential in D2 than in D1 SPNs given the same depolarization magnitude, whereas in KOs this discrepancy is absent. ***E***, ***F***, With equal depolarization magnitude, BLA→D1 SPNs but not in BLA→D2 SPNs synapses exhibit increased probability of firing in FXS mice compared with that in controls. ***G***, ***H***, D2 SPNs exhibit a higher propensity for firing compared with D1 SPNs under equivalent levels of BLA→NAcC optical stimulation in both WT and KO mice. ***I***, ***J***, In the absence of FMRP, both D1 and D2 SPNs show a higher probability of firing than control counterparts under the same level of BLA optical stimulation. ***C–J***, Data are presented as nonlinear fitting regression curves ±95% CI in the *XY* plot. *F* test. Arrows with asterisks indicate statistical difference ($p < 0.05$) between half-maximal firing probability. WT D1 SPNs $N = 6$ ($n = 8$) in dark blue, WT D2 SPNs $N = 5$ ($n = 8$) in light blue, KO D1 SPNs $N = 6$ ($n = 6$) in dark orange, KO D2 SPNs $N = 6$ ($n = 8$) in light orange. Full statistics are provided in Extended Data Tables 5-1 and 5-2.

The increased synaptic transmission to D2 SPNs is not due to altered glutamate release

The observation that different inputs to the NAcC exhibit a similar selective increase in synaptic transmission at their synapses with D2 SPNs, but not with D1 SPNs (Figs. 2, 3), raises the possibility of a shared underlying mechanism. To explore potential presynaptic mechanisms, we investigated if the release probability is changed in both BLA and PFC inputs onto SPNs, assessing synapse-specific PPR. For both inputs, the PPR was consistent across genotypes and cell types (Fig. 6, Extended Data Tables 6-1, 6-2). Consequently, this implies that the altered synaptic transmission observed in BLA→D2 SPNs and PFC→D2 SPNs connections in FXS mice is not associated with changes in the probability of glutamate release at these synapses.

Uncovering postsynaptic alterations in FXS: dendritic spine changes in D2, but not D1, SPNs

Given that the increase in synaptic transmission observed in FXS at the PFC and BLA onto D2 SPNs cannot be attributed to an elevation in presynaptic glutamate release (Fig. 6), we investigated potential postsynaptic mechanisms. Specifically, we compared the number and morphology of dendritic spines in D1 and D2

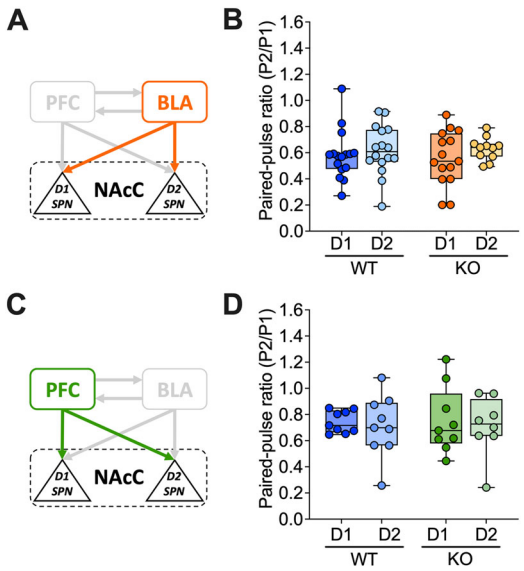

Figure 6. The lack of FMRP has no effect on the release probability of PFC/BLA→NAcC glutamatergic synapses. ***A***, ***C***, Schematic representation illustrating the interconnections between PFC-BLA-NAcC and emphasizing the specific PFC/BLA-NAcC (D1/D2 SPNs) pathways under scrutiny. ***B***, ***D***, FMRP absence does not impact PPR at the synapses of BLA (***B***) and PFC (***D***) with D1 and D2 SPNs. PPR was measured as the ratio of P2/P1 amplitudes evoked at 50 ms intervals. A single dot represents an individual mouse. Data are shown as the min. to max. box plot with median and 25–75 percentile. Two-way ANOVA followed by Tukey's multiple-comparison test. ***B***, WT D1 SPNs $N = 16$ ($n = 19$) in dark blue, WT D2 SPNs $N = 16$ ($n = 20$) in light blue, KO D1 SPNs $N = 15$ ($n = 17$) in dark orange, KO D2 SPNs $N = 11$ ($n = 13$) in light orange. ***D***, WT D1 SPNs $N = 9$ ($n = 10$) in dark blue, WT D2 SPNs $N = 9$ ($n = 10$) in light blue, KO D1 SPNs $N = 9$ ($n = 10$) in dark green, KO D2 SPNs $N = 8$ ($n = 11$) in light green. Full statistics are provided in Extended Data Tables 6-1 and 6-2.

SPNs (Fig. 7). Notably, there were no discernible differences in the density, length, or volume of dendritic spines in D1 SPNs between *Fmr1* WT and KO mice (Fig. 7*A–C*, Extended Data Table 7-1). However, in D2 SPNs, the absence of FMRP resulted in a significant increase in spine density and a reduction in spine length, while the spine volume remained unchanged (Fig. 7*D–F*, Extended Data Table 7-2). These findings indicate that the absence of FMRP selectively induces alterations in the number and morphology of dendritic spines in D2 SPNs, perhaps suggesting a potential postsynaptic mechanism underlying the observed increase in synaptic strength in these neurons.

Within the BLA-PFC-NAcC network, LTD is solely impaired at BLA→D1 SPN synapses in FXS mice

Defective synaptic plasticity, including LTD in the NAcC, is a characteristic feature of a brain lacking FMRP (Jung et al., 2012). However, it is currently unclear whether these LTD deficits are generalized throughout the NAcC or if they are specific to certain inputs. To shed light on the underlying mechanisms of synaptic dysfunction in FXS, LTD was evaluated at the reciprocal PFC↔BLA connection and their respective inputs to the NAcC (Fig. 8). The 10′–10 Hz optical stimulation triggered equal LTD in both *Fmr1* WT and KO mice at both PFC→BLA and BLA→PFC synapses (Fig. 8*A–F*, Extended Data Table 8-1). Conversely, LTD was not observed in PFC→NAcC synapses in either control or FXS mice (Fig. 8*G–I*, Extended Data Table 8-1). The BLA→NAcC pathway exhibits endocannabinoid-mediated long–term depression (eCB-LTD) of synaptic transmission, in WT but not FXS mice (Fig. 8*J–L*, Extended Data Table 8-1). To investigate the cellular specificity of this phenomenon, we examined the disambiguated BLA-SPNs synapses using the whole-cell

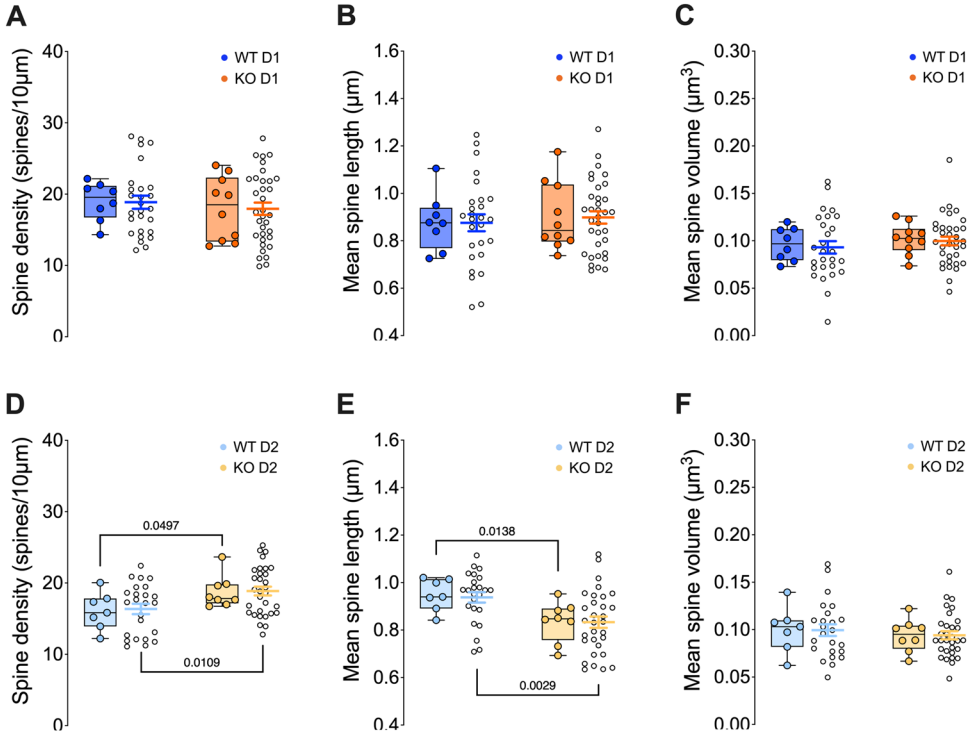

Figure 7. Specific altered spine morphology in D2 SPNs without FMRP: increased spine density and decreased spine length. ***A–C***, The density (***A***), length (***B***), and volume (***C***) of dendritic spines in D1 SPNs show no differences between *Fmr1* WT and KO. ***D–F***, In contrast, the absence of FMRP in D2 SPNs leads to an increase in spine density (***D***), a decrease in spine length (***E***), with no alterations in spine volume (***F***). ***A–F***, The data are presented in two formats: First, in the form of box plots that display the minimum to maximum range, along with the median and the 25th to 75th percentile. Each individual dot on the plot corresponds to a cell (N). Second, the data are represented in a flanked scattered dot plot, where each dot represents a dendrite (n). The mean value is indicated by the dot's position, and the error bars display the standard error of the mean (SEM). Unpaired t tests. P values <0.05 are displayed in graphs. WT D1 SPNs $N = 8$ ($n = 27$) in dark blue, WT D2 SPNs $N = 7$ ($n = 24$) in light blue, KO D1 SPNs $N = 10$ ($n = 34$) in dark orange, KO D2 SPNs $N = 8$ ($n = 31$) in light orange. Full statistics are provided in Extended Data Tables 7-1 and 7-2.

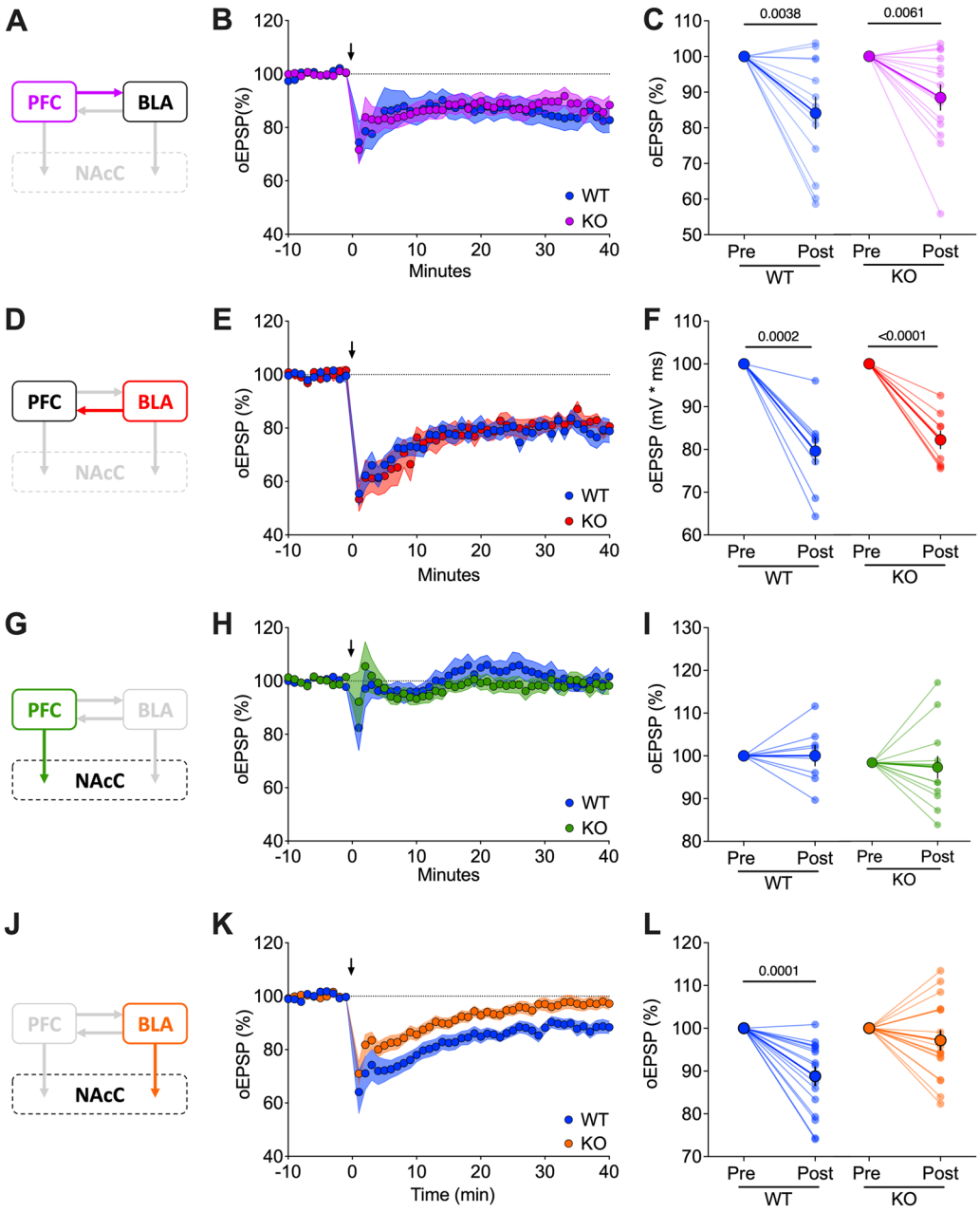

Figure 8. LTD is impaired in the BLA→NAcC synapses of FXS mice. ***A***, ***D***, ***G***, ***J***, Schematic representation of the interconnections between PFC, BLA, and NAcC with the individual pathways examined highlighted. ***B***, ***C***, ***E***, ***F***, ***H***, ***I***, ***K***, ***L***, In FXS mice, the absence of FMRP does not impact LTD in the PFC→BLA (***B***, ***C***) and BLA→PFC (***E***, ***F***) connections while impairing that of the BLA→NAcC (***K***, ***L***) synapses. PFC→NAcC connections does not express LTD in both control and FXS mice (***H***, ***I***). ***B***, ***E***, ***H***, ***K***, Average time courses of mean oEPSPs illustrating the effect of 10′–10 Hz stimulation (indicated by the arrow) on synaptic transmission. A single dot represents group mean value at that time point. Data are shown as mean ± SEM in the *XY* plot. ***C***, ***F***, ***I***, ***L***, Data are shown as pre-post individual experiments and group average ± SEM. Paired *t* tests. *P* values <0.05 displayed in graphs. ***B***, ***C***, WT $N = 13$ in blue, KO $N = 12$ in purple. ***E***, ***F***, WT $N = 9$ in blue, KO $N = 9$ in red. ***H***, ***I***, WT $N = 8$ in blue, KO $N = 13$ in green. ***K***, ***L***, WT $N = 16$ in blue, KO $N = 17$ in orange. Full statistics are provided in Extended Data Table 8-1.

configuration (Fig. 9). In WT mice, both BLA→D1 SPNs and BLA→D2 SPN synapses exhibited eCB-LTD (Fig. 9*D*, Extended Data Table 9-1). However, FMRP-deficient mice showed a deficit in plasticity specifically in the BLA→D1 SPNs synapses (Fig. 9*E*, Extended Data Table 9-1). Collectively, these findings show that in FXS mice, eCB-LTD deficits are specific to BLA→ D1 SPN connections.

Discussion

In this study, we investigated the impact of FXS on the excitatory network involving the PFC, BLA, and NAcC. Overall, the results show that while optogenetically defined reciprocal connections between the PFC and the BLA remained unchanged, the strength of excitatory synaptic transmission from either the PFC or the BLA to the NAcC was enhanced in FXS mice, in a target cell-specific manner. We propose that FXS-induced alterations in synaptic transmission and plasticity within this network may contribute to the specific behavioral and emotional phenotypes observed in FXS individuals.

To understand the underlying mechanisms contributing to the altered synapse-specific transmission, we aimed to distinguish between pre- and postsynaptic factors. The enhancement of both PFC and BLA glutamatergic inputs onto NAcC SPNs,

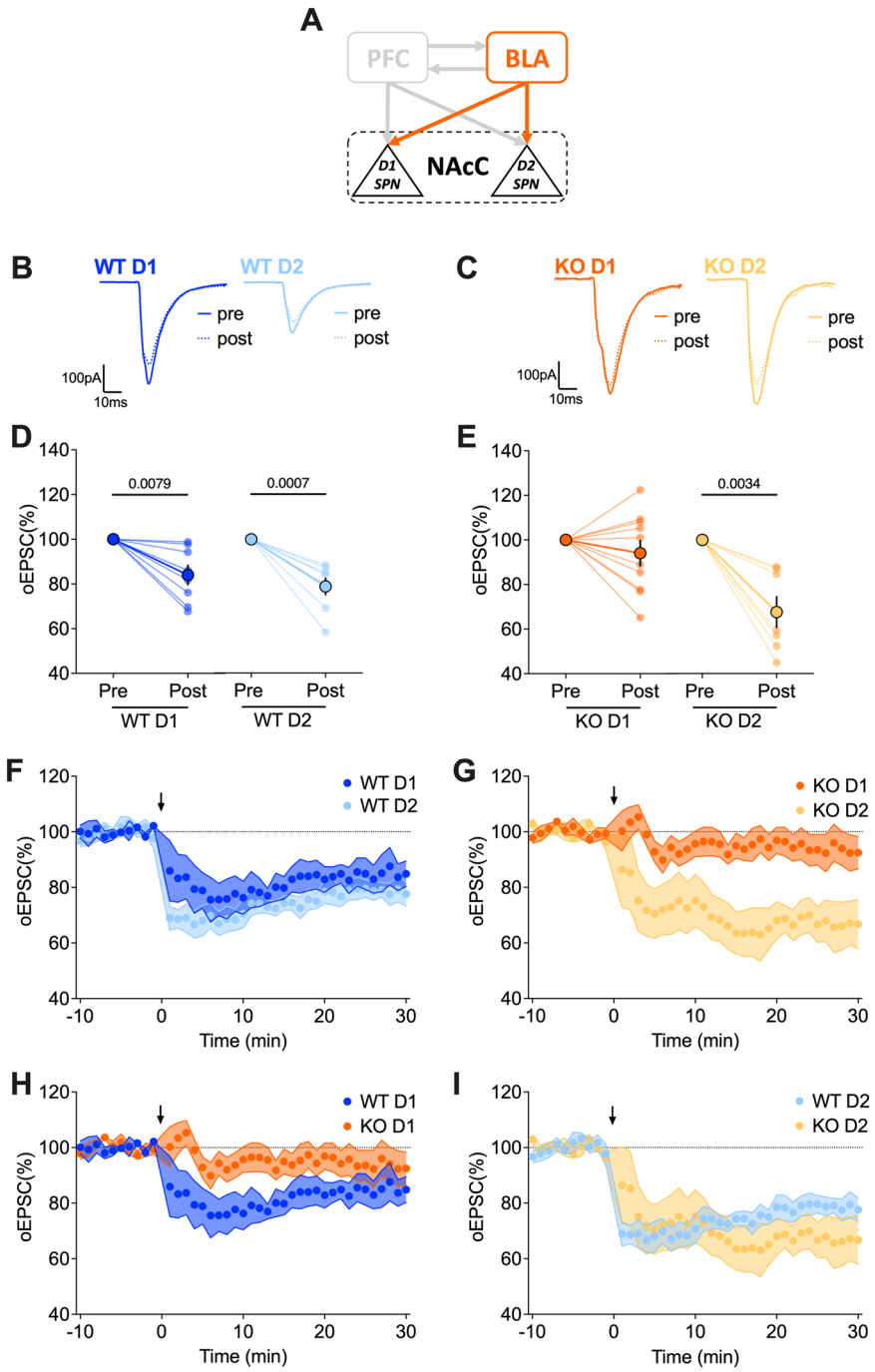

Figure 9. Lack of LTD in FXS mice is specifically observed in the BLA→D1 SPN pathway. ***A***, Schematic representation illustrating the interconnections between PFC-BLA-NAcC and emphasizing the specific BLA-NAcC (D1/D2 SPNs) pathway under scrutiny. ***B***, ***C***, Example traces illustrate the difference between the baseline (solid line) and the response 20–30 min after 10′–10 Hz stimulation (dashed line). ***D***, ***E***, Pre-post analyses comparing oEPSCs at the baseline and 20–30 min after 10′–10 Hz stimulation reveal that LTD is specifically absent in BLA→D1 SPN synapses of *Fmr1* KO mice. ***F–I***, Average time courses of mean oEPSCs demonstrate the LTD induced by 10′–10 Hz stimulation (indicated by the arrow) at BLA-NAcC synapses per genotype (***G***, ***H***) and cell type (***I***, ***J***). ***D***, ***E***, Data are shown as pre-post individual experiments and group average ± SEM. Paired *t* test. *P* values <0.05 displayed in graphs. ***F–I***, A single dot represents group mean value at that time point. Data are presented as mean ± SEM in an *XY* plot. ***D–I***, WT D1 SPNs $N = 8$ ($n = 9$) in dark blue, WT D2 SPNs $N = 8$ ($n = 9$) in light blue, KO D1 SPNs $N = 10$ ($n = 11$) in dark orange, KO D2 SPNs $N = 7$ ($n = 8$) in light orange. Full statistics are provided in Extended Data Table 9-1.

paralleled by an increase in both AMPAR and NMDAR currents at BLA→D2 SPN synapses, suggested postsynaptic changes. PPR measurements favored the idea that the absence of FMRP did not grossly affect presynaptic release probability at either PFC→NAcC or BLA→NAcC glutamatergic synapses.

Our study builds upon and significantly extends previous morphological findings in FXS models, providing a more comprehensive understanding of the complex neural mechanisms underlying this disorder. Previous results in FXS models showed morphological and quantitative alterations of dendritic spines in different brain areas (He and Portera-Cailliau, 2013), including an increase in the density and length of spines in NAcC SPNs (Neuhofer et al., 2015). Identifying SPNs' subtypes, we observed a significant increase in spine density and a

reduction in spine length in D2 SPNs, but not D1 SPNs, in FXS mice. Together with our previous report that the absence of FMRP transformed the intrinsic properties of D1 and D2 SPNs in a cell-specific manner (Giua et al., 2023), the current electrophysiological and morphological data support the idea that cell-specific postsynaptic alterations in the NAcC are essential contributors of the current phenotype. The coincidence of increased synaptic strength with elevated postsynaptic dendritic spine density in the absence of FMRP in BLA/PFC→D2 SPN suggests a plausible mechanism: the increased spine density may contribute to the enhanced synaptic strength by providing more postsynaptic sites for neurotransmitter release to act on. However, this hypothesis requires further investigation to be validated. Interestingly, the lack of changes in PPR may indicate that these alterations are, at least in part, compensatory or homeostatic in nature, serving to maintain the overall stability and balance of the neuronal network. This complex interplay between synaptic strength, spine morphology, and network stability highlights the need for further research to fully elucidate the underlying mechanisms driving the FXS phenotype.

Heightened transmission between the BLA and NAcC may contribute to the altered social behaviors and increased susceptibility to stress observed in FXS. In typical animals, activation of this pathway leads to reduced motivation for social interaction, decreased social preference, and increased social avoidance (Folkes et al., 2020). Conversely, inhibiting this pathway in the context of *Shank3* has been shown to restore social avoidance (Folkes et al., 2020). Therefore, the strength of BLA→NAcC synaptic transmission could serve as a crucial regulator of social approach/avoidance behaviors in both healthy and FXS conditions.

Our observation that the increased glutamatergic transmission in FXS mice specifically occurs at synapses onto D2 SPNs aligns with previous research demonstrating the significant role of NAcC D2 SPNs in regulating stress susceptibility (Hamilton et al., 2018). Specifically, the heightened activity in BLA→D2 SPNs is a characteristic feature of mice susceptible to social stress (Shen et al., 2019). Hence, the increased synaptic transmission strength in BLA→D2 SPNs reported in our study may contribute to the heightened susceptibility to stressors observed in individuals with FXS.

Glutamatergic BLA neurons that project to the NAcC exhibit a high level of segregation, forming two distinct parallel pathways: one composed of non-cholecystokinin (CCK) neurons projecting onto D1 SPNs and the other comprising CCK neurons projecting onto D2 SPNs (Shen et al., 2019). This architectural organization could account for the selectivity we observed in the alterations of synaptic transmission, as the changes might be specific to these two different parallel projections from the BLA to the NAcC. Furthermore, in vivo activation of the CCK^{BLA}–$D2^{NAcC}$ pathway has an aversive effect in mice and that social stress selectively activates the CCK^{BLA}–$D2^{NAcC}$ circuit (Shen et al., 2019). Thus, the increased strength of this specific connection in FXS mice may contribute to the aversive nuances of FXS behavior in stressful or social situations.

Hyperexcitability of the BLA is frequently observed in neuropsychiatric and neurodevelopmental disorders characterized by heightened stress susceptibility, enhanced emotional reactivity, or increased social withdrawal responses (Prager et al., 2016; Sharp, 2017). In FXS mice, the local GABAergic circuitry within the BLA undergoes alterations, resulting in hyperexcitability of glutamatergic output neurons (Olmos-Serrano et al., 2010). Thus, the augmented strength of BLA→NAcC transmission observed in the absence of FMRP, as reported in our study, may contribute to the overall hyperexcitability in BLA circuits. This suggests that there might be a lack of homeostatic adaptation mechanisms in place to counterbalance the heightened transmission.

To gain deeper insights into how the excitatory inputs from the BLA are integrated at the postsynaptic level in D1 and D2 SPNs, ES coupling experiments were conducted. The results revealed that both pathways have a higher likelihood of firing in the absence of FMRP due to two distinct yet converging mechanisms. In the case of BLA→D1 SPNs, while the BLA maintains normal synaptic transmission on D1 SPNs in FXS mice, the absence of FMRP results in a decrease in their firing threshold (Giua et al., 2023), thereby facilitating their firing. On the other hand, for BLA→D2 SPNs, although the absence of FMRP does not affect the threshold of D2 SPNs (Giua et al., 2023), the BLA exhibits a stronger excitatory synaptic strength, making it more likely for them to reach their threshold and generate action potentials. Indeed, in FXS mice, both D1 and D2 SPNs achieved a half-maximal probability of firing with lower BLA→NAcC stimulations compared with their WT counterparts. These results support the idea that activation of both D1- and D2-mediated pathways in response to BLA stimulation is significantly more likely in FXS mice.

Previous research had established that a deficiency of FMRP affects synaptic plasticity in the NAcC (Jung et al., 2012; Neuhofer et al., 2015, 2018). A prominent form of plasticity in this brain area is eCB-LTD (Robbe et al., 2002). We previously demonstrated that eCB-LTD is impaired in the NAcC in the absence of FMRP (Jung et al., 2012), contrasting with observations of heightened LTD in the hippocampus of FXS mice (Huber et al., 2002). However, these findings are only apparently discordant since in the hippocampus, LTD relies on Group 1 mGlu receptor-mediated protein synthesis (mGlu receptor-mediated long–term depression, mGluR-LTD), whereas accumbal eCB-LTD operates independently of protein synthesis (Jung et al., 2012) and is instead induced by the retrograde endocannabinoid transmitter, 2-arachidonoyl-sn-glycerol (Jung et al., 2012). Because of these distinct underlying mechanisms, the absence of FMRP affects these two phenomena differently: Firstly, FMRP acts as a translational repressor protein, so its absence results in excessive protein synthesis, thereby increasing mGluR-LTD (Huber et al., 2002). Secondly, FMRP regulates the signalosome connecting mGluR5 to diacylglycerol lipase α, and in its absence, the activation of mGluR5 corresponds to a deficient retrograde release of 2-AG (Jung et al., 2012). In the frame of this study, we inquired whether eCB-LTD deficiency in the NAcC of FXS mice was pathway specific. Our findings reveal that eCB-LTD was selectively impaired in the BLA→NAcC-D1 SPN pathway in FXS. This suggests that FMRP expression is necessary for the proper assembly of the eCB signaling complex at glutamatergic synapses of BLA→D1 SPNs, while it does not appear to be necessary for BLA→D2 SPNs. FMRP is required for the development of cocaine-induced behavioral sensitization, cocaine-related reward learning, and normal NAcC function in these processes (Smith et al., 2014). Additionally, selective deficits in eCB-LTD at accumbal D1 SPNs can lead to the suppression of drug and natural reward responses, as well as the seeking of brain stimulation (Bilbao et al., 2020). Together, our findings suggest that the selective impairment of eCB-LTD in the BLA→NAcC-D1 SPNs pathway is dependent on FMRP expression for proper assembly of the eCB signaling complex at specific glutamatergic synapses and that it may serve as a biological basis for the reward-related behavioral changes observed in FXS.

In conclusion, our study reveals a complex interplay between altered excitatory transmission, synaptic plasticity, and postsynaptic adaptations in the NAcC of FXS mice. These pathway-specific changes, particularly the enhanced BLA→D2 SPN transmission and the selective impairment of eCB-LTD in the BLA→D1 SPN pathway, may serve as the biological basis for the specific behavioral and emotional phenotypes observed in FXS individuals, including heightened stress susceptibility, social withdrawal, and disruptions in reward processing.

Data Availability Statement

All data reported in this paper will be shared by the lead contact upon request. This paper does not report the original code. Any additional information required to reanalyze the data reported in this paper is available from the lead contact upon request.

References

Amadei EA, et al. (2017) Dynamic corticostriatal activity biases social bonding in monogamous female prairie voles. Nature 546:297–301.

Bercovici DA, Princz-Lebel O, Tse MT, Moorman DE, Floresco SB (2018) Optogenetic dissection of temporal dynamics of amygdala-striatal interplay during risk/reward decision making. eNeuro 5:0422-18.

Bilbao A, et al. (2020) Endocannabinoid LTD in accumbal D1 neurons mediates reward-seeking behavior. iScience 23:100951.

Block AE, Dhanji H, Thompson-Tardif SF, Floresco SB (2007) Thalamic-prefrontal cortical-ventral striatal circuitry mediates dissociable components of strategy set shifting. Cereb Cortex 17:1625–1636.

Bromberg-Martin ES, Matsumoto M, Hikosaka O (2010) Dopamine in motivational control: rewarding, aversive, and alerting. Neuron 68:815–834.

Christakou A, Robbins TW, Everitt BJ (2004) Prefrontal cortical-ventral striatal interactions involved in affective modulation of attentional performance: implications for corticostriatal circuit function. J Neurosci 24:773–780.

Contractor A, Klyachko VA, Portera-Cailliau C (2015) Altered neuronal and circuit excitability in fragile X syndrome. Neuron 87:699–715.

Daoudal G, Hanada Y, Debanne D (2002) Bidirectional plasticity of excitatory postsynaptic potential (EPSP)-spike coupling in CA1 hippocampal pyramidal neurons. Proc Natl Acad Sci U S A 99:14512–14517.

Floresco SB (2015) The nucleus accumbens: an interface between cognition, emotion, and action. Annu Rev Psychol 66:25–32.

Folkes OM, et al. (2020) An endocannabinoid-regulated basolateral amygdala-nucleus accumbens circuit modulates sociability. J Clin Invest 130:1728–1742.

Francis TC, et al. (2015) Nucleus accumbens medium spiny neuron subtypes mediate depression-related outcomes to social defeat stress. Biol Psychiatry 77:212–222.

Gagnon D, Petryszyn S, Sanchez MG, Bories C, Beaulieu JM, De Koninck Y, Parent A, Parent M (2017) Striatal neurons expressing D1 and D2 receptors are morphologically distinct and differently affected by dopamine denervation in mice. Sci Rep 7:41432.

Giua G, Lassalle O, Makrini-Maleville L, Valjent E, Chavis P, Manzoni OJJ (2023) Investigating cell-specific effects of FMRP deficiency on spiny projection neurons in a mouse model of fragile X syndrome. Front Cell Neurosci 17:237.

Guily P, Lassalle O, Chavis P, Manzoni OJ (2022) Sex-specific divergent maturational trajectories in the postnatal rat basolateral amygdala. iScience 25:103815.

Hamilton PJ, Burek DJ, Lombroso SI, Neve RL, Robison AJ, Nestler EJ, Heller EA (2018) Cell-type-specific epigenetic editing at the Fosb gene controls susceptibility to social defeat stress. Neuropsychopharmacology 43:272–284.

Hauber W, Sommer S (2009) Prefrontostriatal circuitry regulates effort-related decision making. Cereb Cortex 19:2240–2247.

He CX, Portera-Cailliau C (2013) The trouble with spines in fragile X syndrome: density, maturity and plasticity. Neuroscience 251:120–128.

Huber KM, Gallagher SM, Warren ST, Bear MF (2002) Altered synaptic plasticity in a mouse model of fragile X mental retardation. Proc Natl Acad Sci U S A 99:7746–7750.

Hunter J, Rivero-Arias O, Angelov A, Kim E, Fotheringham I, Leal J (2014) Epidemiology of fragile X syndrome: a systematic review and meta-analysis. Am J Med Genet A 164A:1648–1658.

Iafrati J, Orejarena MJ, Lassalle O, Bouamrane L, Chavis P (2014) Reelin, an extracellular matrix protein linked to early onset psychiatric diseases, drives postnatal development of the prefrontal cortex via GluN2B-NMDARs and the mTOR pathway. Mol Psychiatry 19:417–426.

Jung KM, et al. (2012) Uncoupling of the endocannabinoid signalling complex in a mouse model of fragile X syndrome. Nat Commun 3:1080.

Kasanetz F, Manzoni OJ (2009) Maturation of excitatory synaptic transmission of the rat nucleus accumbens from juvenile to adult. J Neurophysiol 101:2516–2527.

Lafourcade M, Elezgarai I, Mato S, Bakiri Y, Grandes P, Manzoni OJ (2007) Molecular components and functions of the endocannabinoid system in mouse prefrontal cortex. PLoS One 2:e709.

Leduke DO, Borio M, Miranda R, Tye KM (2023) Anxiety and depression: a top-down, bottom-up model of circuit function. Ann N Y Acad Sci 1525: 70–87.

Lobo MK, Nestler EJ (2011) The striatal balancing act in drug addiction: distinct roles of direct and indirect pathway medium spiny neurons. Front Neuroanat 5:41.

Murray EA, Fellows LK (2022) Prefrontal cortex interactions with the amygdala in primates. Neuropsychopharmacology 47:163–179.

Neuhofer D, Henstridge CM, Dudok B, Sepers M, Lassalle O, Katona I, Manzoni OJ (2015) Epidemiology of fragile X syndrome: a systematic review and meta-analysis. Front Cell Neurosci 9:100.

Neuhofer D, Lassalle O, Manzoni OJ (2018) Muscarinic M1 receptor modulation of synaptic plasticity in nucleus accumbens of wild-type and fragile X mice. ACS Chem Neurosci 9:2233–2240.

Olmos-Serrano JL, Paluszkiewicz SM, Martin BS, Kaufmann WE, Corbin JG, Huntsman MM (2010) Defective GABAergic neurotransmission and pharmacological rescue of neuronal hyperexcitability in the amygdala in a mouse model of fragile X syndrome. J Neurosci 30:9929–9938.

Pfaff D, Barbas H (2019) Mechanisms for the approach/avoidance decision applied to autism. Trends Neurosci 42:448–457.

Prager EM, Bergstrom HC, Wynn GH, Braga MFM (2016) The basolateral amygdala γ-aminobutyric acidergic system in health and disease. J Neurosci Res 94:548–567.

Puente N, Cui Y, Lassalle O, Lafourcade M, Georges F, Venance L, Grandes P, Manzoni OJ (2011) Polymodal activation of the endocannabinoid system in the extended amygdala. Nat Neurosci 14:1542–1547.

Robbe D, Kopf M, Remaury A, Bockaert J, Manzoni OJ (2002) Endogenous cannabinoids mediate long-term synaptic depression in the nucleus accumbens. Proc Natl Acad Sci U S A 99:8384–8388.

Sharp BM (2017) Basolateral amygdala and stress-induced hyperexcitability affect motivated behaviors and addiction. Transl Psychiatry 7:e1194.

Shen CJ, et al. (2019) Cannabinoid CB1 receptors in the amygdalar cholecystokinin glutamatergic afferents to nucleus accumbens modulate depressive-like behavior. Nat Med 25:337–349.

Smith LN, et al. (2014) Fragile X mental retardation protein regulates synaptic and behavioral plasticity to repeated cocaine administration. Neuron 82: 645–658.

Supekar K, Kochalka J, Schaer M, Wakeman H, Qin S, Padmanabhan A, Menon V (2018) Deficits in mesolimbic reward pathway underlie social interaction impairments in children with autism. Brain 141:2795–2805.

Vialou V, et al. (2014) Prefrontal cortical circuit for depression- and anxiety-related behaviors mediated by cholecystokinin: role of ΔFosB. J Neurosci 34:3878–3887.

Wiśniowiecka-Kowalnik B, Nowakowska BA (2019) Genetics and epigenetics of autism spectrum disorder-current evidence in the field. J Appl Genet 60:37–47.

Yizhar O, Fenno LE, Davidson TJ, Mogri M, Deisseroth K (2011) Optogenetics in neural systems. Neuron 71:9–34.